Vol. 82 (1992) *ACTA PHYSICA POLONICA A* No 4

Proceedings of the XXI International School of Semiconducting Compounds, Jaszowiec 1992

POINT-CONTACT SPECTROSCOPY

A.G.M. JANSEN

Max-Planck-Institut für Festkörperforschung, Hochfeld-Magnetlabor
B.P.166, 38042 Grenoble Cedex 9, France

In a small metallic constriction ("point contact") the transport of electrons is ballistic. The applied voltage V tunes a well-defined non-equilibrium energy eV of electrons. The nonlinear current–voltage characteristics can be used to perform energy-resolved spectroscopy of the inelastic scattering of electrons with elementary excitations in metal (e.g. phonons, magnons, crystal-field levels, paramagnetic impurities). The basic elements of the point-contact method and its applications will be discussed. In recent point-contact experiments the observed phenomena (weak localization, resistance fluctuations) need a description that goes beyond the classical Boltzmann approach of electronic transport in a point contact. In analogy to observed effects in the diffusive transport in mesoscopic systems, these phenomena are explained by considering quantum-interference effects in the ballistic transport near the contact region related to the wave character of the electrons.

PACS numbers: 72.10.–d, 73.40.Jn

For a macroscopic sample in an applied electric field E, the acceleration of the electrons during a mean free path ℓ is only a very small perturbation with respect to the thermal excitations at a temperature T (i.e $eE\ell < k_BT$). This thermal equilibrium of the electronic system in an applied electric field is one of the reasons for the linear relation between the current density and the electric field as given by Ohm's law. For a small metallic constriction (size of the constriction small compared to the electronic mean free path), all electrons passing the contact gain a well-defined energy eV given by the applied voltage V. In such a ballistic point contact the electronic system is out of equilibrium with an excess energy eV that can be bigger than k_BT. Sharvin [1] proposed the realization of this ballistic transport mechanism in metallic point contacts. In his pioneering experiments on shorted tunnel junctions, Yanson [2] observed nonlinearitics in thc currcnt–voltage characteristics at applied voltages corresponding to the bulk phonon frequencies of the studied material. These experiments revealed the usefullness of point contacts for energy-resolved spectroscopy of electronic scattering with quasi-particle excitations (e.g. phonons) by tuning the applied voltage over the metal contact.

The method of point-contact spectroscopy will be discussed and examples of point-contact investigations will be given. The given description of the electronic transport in a point contact is based on a classical solution of the Boltzmann transport equation. In anology to the phenomena of weak-localization and conductance

fluctuations in (mesoscopic) systems with diffusive transport, recent experiments show the importance of quantum-interference effects for the ballistic transport of electrons in a point contact.

1. Method

Over the years several reviews [3] have appeared dealing with various aspects (both theory and experiment) of the point-contact technique. Recently the first conference on point-contact spectroscopy [4] was held in Kharkov, Ukraine. In this section only the main lines of the point-contact technique will be given. A more extensive information on the theory and the experimental results can be found in the given references.

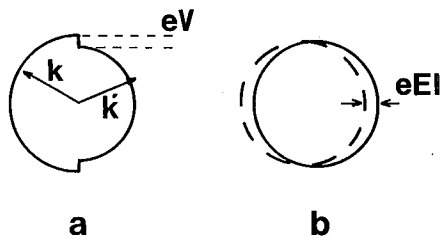

Fig. 1. The Sharvin distribution (a) of the electrons in the center of a ballistic point contact, schematically showing the energy difference eV between electrons coming from the low potential side of the contact and those from the high potential side. The arrows indicate an inelastic backscattering process from state k to k'. The shifted Fermi sphere (b) obtained from classical transport theory for a bulk system in the relaxation-time approximation for an electric field E and a scattering length ℓ.

An important parameter to characterize the electronic transport in a metallic constriction is given by the ratio between the electron mean free path ℓ and the contact radius a (the contact is represented by a circular conducting hole in an insulating screen between two metal parts). For large contacts ($\ell < a$), the transport through the contact is a diffusive process. Maxwell [5] treated this problem using Ohm's law and solving the Poisson equation for the electric field in the contact geometry. He obtained for the contact resistance $R_{\mathrm{M}} = \rho/2a$, which result can be easily seen as the resistance of a sample (area a^2, length a) with resistivity ρ. For small contacts ($\ell > a$), the transport of the electrons is ballistic. For an applied voltage V over the contact, the angular distribution of the electrochemical potential contains different parts with an energy difference eV depending on the starting point (high or low potential side of the contact) of the electron trajectories. In Fig. 1a we have schematically shown the resulting half spheres with energy difference eV for the non-equilibrium distribution of the electrons at the center of the contact. By intergrating the velocity component $v_\perp$ perpendicular to the contact surface over the distorted Fermi sphere S (Fig. 1a), one can calculate the current $I_0 = 2e\pi a^2 \int_S v_\perp \mathrm{d}^3k/(2\pi)^3$ through the contact area πa^2. Using the

Drude relation of the electrical resistivity ρ, one obtains the contact resistance $R_{\mathrm{Sh}} = 4\rho\ell/3\pi a^2$ [1]. The Sharvin resistance for a clean contact depends only on the contact surface and the Fermi surface, and is independent of the material purity (in the Drude model for free electrons $\rho\ell$ equals mv_{F}/ne^2 with Fermi velocity v_{F} and electron concentration n).

In an alternative way the contact resistance can be described in the Landauer transmission formulation [6] for ballistic transport. In a multi-channel formula the conductance G of a sample can be written as

$$G = (2e^2/h) \sum_{\alpha,\beta=1}^{N} | t_{\alpha\beta} |^2, \tag{1}$$

where $2e^2/h$ is the conductance per channel (including spin degeneracy) and $| t_{\alpha\beta} |^2$ the transmission probability between incoming channels α and outgoing channels β. In the ballistic limit without scattering $t_{\alpha\beta}$ is equal to $\delta_{\alpha\beta}$. Summing in Eq. (1) over the total number of channels $N = a^2k_{\mathrm{F}}^2/4$ through the contact leads to the above given expression for the Sharvin resistance $R_{\mathrm{Sh}} = 1/G_{\mathrm{Sh}}$ for a clean contact.

For the total range of values for the ratio a/ℓ, an interpolation formula between the two limiting regimes can be taken for the contact resistance

$$R_{\mathrm{contact}} \simeq R_{\mathrm{Sh}} + R_{\mathrm{M}} \simeq \frac{\rho\ell}{a^2}(1 + \frac{a}{\ell}). \tag{2}$$

It can be readily seen that the scattering-dependent Maxwell term in the resistance corresponds to a perturbation of the scattering-independent Sharvin term (of order $a/\ell < 1$ for a pure contact). Just this second term in Eq. (2) changes the contact resistances at an applied voltage via the energy-dependent scattering of the non-equilibrium distribution of the electrons.

To support the phenomenological approach of the above given interpolation formula, the Boltzmann transport equation of the point-contact problem has to be solved under the appropriate boundary conditions (applied voltage over the constriction and local charge neutrality). Without the scattering term in the Boltzmann equation the zeroth order contribution I_0 to the current is found from the Sharvin distribution of the electrons near the contact (see Fig. 1a). Adding inelastic electron transitions, like the one sketched in Fig. 1a, yields a negative correction I_1 to the current which depends on the energy-dependent scattering length $\ell(\epsilon)$ for an electron with non-equilibrium energy ϵ above the Fermi level. Using the path integral method for the electron trajectories to solve the Boltzmann equation with scattering included, this negative backflow current I_1 is given by (apart from a numerical factor)

$$I_1 \approx -ea^2N_0v_{\mathrm{F}} \int_0^{eV} \frac{a}{\ell(\epsilon)} \mathrm{d}\epsilon. \tag{3}$$

N_0 is the density of states of the electrons at the Fermi surface. Comparing I_0 and I_1, the expansion in $a/\ell(\epsilon)$ can be seen. The inelastic scattering rate $1/\tau(\epsilon) = v_{\mathrm{F}}/\ell(\epsilon)$ follows from a Golden Rule argument yielding

$$\frac{1}{\tau(eV)} = \frac{2\pi}{\hbar} \int_0^{eV} \alpha^2F_{\mathrm{p}}(\epsilon)\mathrm{d}\epsilon, \tag{4}$$

with the spectral function

$$\alpha^2F(\epsilon)_\mathrm{p} = \frac{N_0}{32\pi^2}\int \mathrm{d}^2n \int \mathrm{d}^2n' \mid g_{n,n'} \mid^2 K_{n,n'}\delta(\epsilon - \hbar\omega_{n,n'}) \tag{5}$$

for e.g. the electron–phonon interaction. The electron–phonon-interaction function α^2F_p contains a matrix element $g_{n,n'}$ with an efficiency factor $K_{n,n'}$ for a backscattering process from unit vector n to n' on the Fermi sphere under the emission of a phonon with energy $\hbar\omega_{n,n'}$. From Eq. (3) it follows that the change in the first derivative $\mathrm{d}I/\mathrm{d}V$ is directly proportional to the inelastic scattering rate for the relaxation of an electron with energy eV above the Fermi level in a cold environment with the same temperature as the bath temperature ($eV > k_\mathrm{B}T$). As a final result one finds for the second derivative of the current–voltage characteristic

$$\mathrm{d}^2I/\mathrm{d}V^2 = -\frac{16\pi}{3}\frac{e^3a^3}{\hbar}N_0\alpha^2F_\mathrm{p}(eV), \tag{6}$$

where the numerical factor is given for free electrons and a circular orifice. The last equation shows the direct relation between the measured nonlinearity of the I–V curve of a point contact and the Eliashberg function α^2F_p for the electron–phonon interaction (slightly modified because of the efficiency factor K in the point-contact geometry). Here an example has been given for the inelastic scattering of the electrons with phonons, but the result can be equally well applied to any other inelastic scattering process, characterized by its own spectral function.

2. Applications

In order to perform point-contact spectroscopy, i.e. inelastic scattering length large compared to the contact diameter, the size of the contact has to be typically of the order of 10 nm. The very first spectroscopic investigations with point contacts have been done by Yanson [2] on evaporated tunnel junctions with a short-circuit in the insulating barrier. By extending the experimental technique to mechanically adjustable contacts in a spear-anvil geometry [7], many metals (even single crystals and compounds) could be studied in a rather easy way. Recently, contacts could be fabricated by means of lithography at a nanometer scale [8]. A single hole is patterned in an insulating silicon nitride membrane using e-beam lithography and dry etching. The final point-contact device is produced by the evaporation of a metal layer on both sides of the membrane. This last method results in small and stable contacts of well-defined geometry.

In Fig. 2 the current–voltage characteristics are given for a Cu–Cu pressure-type contact at liquid helium temperatures. The differential resistance $\mathrm{d}V/\mathrm{d}I$ shows an increase at voltages corresponding to the bulk phonon frequencies. In the second-derivative signal $\mathrm{d}^2V/\mathrm{d}I^2$ the structure of the transverse phonons (16–20 meV) and longitudinal phonons (30 meV) can be clearly recognized. The second derivative signal, proportional to the electron–phonon-interaction function α^2F, can be compared with the phonon density of states F as measured by means of inelastic neutron scattering. For the case of Cu, it follows from this comparison that the transverse phonons couple stronger than the longitudinal phonons with the electrons. This phenomenon, also observed in other noble metals and transition metals, can be ascribed to the importance of umklapp scattering processes.

On the other hand for simple metals with a spherical Fermi surface, like the alkali metals Li, K and Na, the coupling with longitudinal phonons is found to be more important. The point-contact technique is the only method which gives such a detailed information on the energy dependence of the electron–phonon interaction in normal metals. For superconductors, the spectral function α^2F can be recovered from the measured tunneling conductance (proportional to the density of states of the quasi-particle excitations in the superconductor) by an iterative solution of the coupled Eliashberg equations describing superconductivity with strong electron–phonon interaction [9].

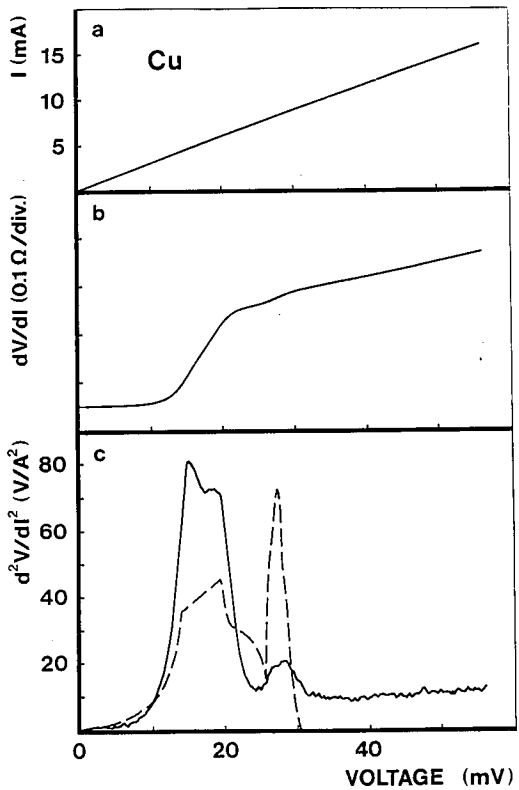

Fig. 2. Current I, differential resistance $\mathrm{d}V/\mathrm{d}I$ and second derivative $\mathrm{d}^2V/\mathrm{d}I^2$ as a function of the applied voltage for a pressure-type Cu–Cu point contact at 1.5 K. The second derivative signal is proportional to the Eliashberg function α^2F for the electron–phonon interaction and can be compared with the phonon density of states F obtained by inelastic neutron scattering (dashed curve).

Many metals have been studied using the point-contact technique [3]. Point-contact spectroscopy has been especially successful for an investigation of the electron–phonon interaction. However, other interaction mechanisms can be studied as well. In point-contact experiments with Gd, Tb and Ho [10], the interaction

between electrons and magnons has been investigated. The electronic scattering on paramagnetic impurities (Kondo effect, spin-glass regime) has been observed in point-contact experiments with noble metals diluted with paramagnetic impurities [11]. In the following an example of the study of crystal-field levels in $PrNi_5$ will be given [12].

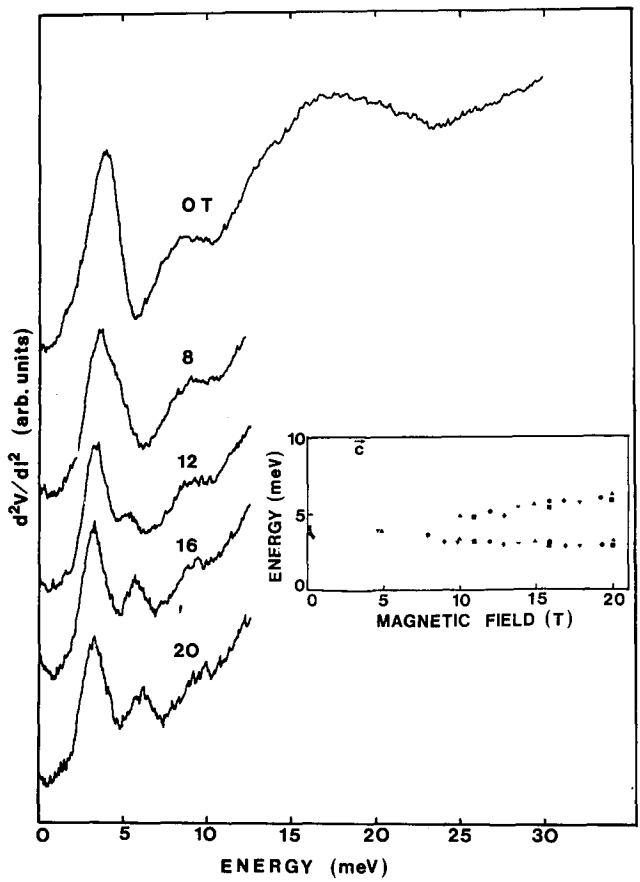

Fig. 3. The second derivative spectra of a $PrNi_5$–Cu point contact at 1.5 K for different values of the magnetic field applied parallelly to the c-axis of $PrNi_5$. The inset shows the Zeeman splitting of the crystal-field level at 4 meV obtained from the spectra (different symbols for different point contacts).

For the case of the Pr^{3+} ion in $PrNi_5$, the ninefold degenerate multiplet of Pr^{3+} is split into 3 singlet and 3 doublet states by the crystal field of the hexagonal lattice. Via the exchange interaction $\boldsymbol{J}\cdot\boldsymbol{s}$ between the angular momentum $\boldsymbol{J}$ of an ion and the spin operator $\boldsymbol{s}$, the accelerated electrons in the point-contact region can excite the Pr^{3+} from the ground state to higher states in the crystal-field-level scheme. In Fig. 3 the point-contact spectrum is given for a Cu electrode pressed

against a single crystal of $PrNi_5$ for various values of the applied magnetic field parallel to the *c*-axis. The structure in the spectra at zero magnetic field is due to the spontaneous emission of phonons and to the excitation of the Pr^{3+} ion from the ground state by the accelerated electrons. The peak around 4 meV is due to the allowed crystal-field transition with the lowest energy. The structure at higher applied voltages has its origine in both phonons and crystal-field transitions.

In an applied magnetic field, the point-contact spectra measure directly the Zeeman splitting of the crystal-field levels (see Fig. 3 for magnetic fields up to 20 T). For the magnetic field parallel to the *c*-axis only the splitting of a doublet is observed. For the other orientations of the magnetic field, a more complex Zeeman splitting is observed resulting from allowed transitions which are forbidden in zero field. The Heisenberg exchange interaction $\boldsymbol{B} \cdot \boldsymbol{J}$ (magnetic field $\boldsymbol{B}$ and total angular momentum $\boldsymbol{J}$ of the ion) in the Zeeman term of the Hamiltonian yields solutions of the Zeeman splitting of the crystal-field levels which explain the observed dependence on the orientation of the magnetic field with respect to the single crystal. These point-contact experiments yield especially new information about the crystal-field energy levels to which the transition from the ground state is forbidden in zero magnetic field [12].

Point-contact spectroscopy has been mostly applied to metallic systems, and only a few applications exist on semiconducting samples [13, 14]. Apart from the surface condition of the sample (only a volume of roughly 10 nm is probed by the contact), a more principal limitation for the spectroscopic application of point contacts is given by the condition for ballistic transport: inelastic scattering length $\ell(\epsilon) >$ contact radius a. For the case that the impurity mean free path $\ell_i < \ell(\epsilon)$, this condition can be relaxed to $\Lambda(\epsilon) > a$. The inelastic diffusion length $\Lambda(\epsilon) = [\ell_i \ell(\epsilon)]^{1/2}$ describes then the characteristic length for energy relaxation. In the dirty limit ($\ell(\epsilon), \Lambda(\epsilon) < a$), the applied voltage over the contact no longer defines the non-equilibrium distribution of the electrons. Many inelastic scattering processes in the contact region will locally heat the contact. The voltage dependence of the contact resistance $R_M(V)$ resembles the temperature dependence of the resistivity $\rho(T)$. In point-contact experiments with ferromagnetic Co, Fe and Ni, the center of the contact has been tuned through the Curie temperature by means of the applied voltage [15].

3. Semi-metals

The point contacts with As [16], Sb [17] and graphite [18] show also structure in the second derivative spectra related to the electron–phonon interaction. However, in these semi-metals often the d^2V/dI^2 signal is negative corresponding to a decrease of the contact resistance at the voltages of the characteristic phonon frequencies instead of the resistance increase as usually observed in point-contact spectroscopy. In Fig. 4 an example of this remarkable phenomenon is given for spectra obtained with contacts between Cu and As. Because of the smaller Fermi velocity of the semi-metal As only spectroscopic features of As are visible in the heterocontacts. For this semi-metal, contacts are obtained both with positive and negative d^2V/dI^2 signals at the corresponding phonon energies. The two peaks

(or valleys) at 10–15 meV and at 25 meV can be ascribed to the acoustic and optic-phonon branches. Where freshly adjusted contacts show positive d^2V/dI^2 signals, repeatedly mechanical adjustment of the contact results in the occurence of negative d^2V/dI^2 signals. To explain this phenomenon the local purity in the contact region has to be considered.

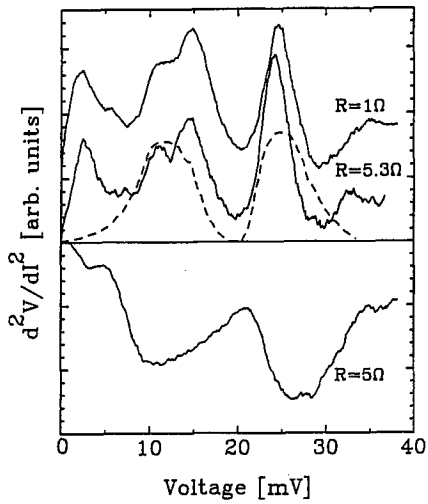

Fig. 4. The second derivative spectra of As–Cu point contacts at 1.5 K with the indicated values of the contact resistance. The structure in both negative and positive spectra can be compared with the phonon density of states of As (dashed curve).

For a pressure-type contact, the local deformation in the contact region yields a smaller elastic mean free path ℓ_i inside the contact area. For semi-metals, the elastic mean free path can reach a value comparable with the de Broglie wavelength λ_{dB} ($\simeq$ 2 nm for As). In this case the wave character of the electrons cannot be neglected in the electronic transport. The interference of electronic waves between time-reversed complementary trajectories of the scattered electrons leads to an enhanced backscattering in the electronic transport. In a disordered bulk system this phenomenon is known as weak localization [19] and leads to an enhanced resistivity which can be suppressed by increasing the temperature, thereby destroying the phase-coherent transport with inelastic scattering events. For the case of a point-contact, inelastic phonon-emission processes also destroy the interference effects leading to a decrease in the contact resistance at the phonon energies. Provided that the inelastic diffusion length $\Lambda_\epsilon = (\ell_i \ell_\epsilon)^{1/2}$ is larger than the contact diameter, the excess energy of the electrons is still determined by the voltage across the contact. Thus point-contact spectroscopy can be done in disordered metals, where quantum localization is important.

In an applied magnetic field the observed magnetoresistance reflects the difference in transport regime between contacts with positive and negative spectra [16]. Contacts with a positive spectrum reveal a positive point-contact magnetore-

sistance pointing to metallic transport. The observed negative magnetoresistance in contacts with negative spectra agrees with the localization model for the electronic transport in the dirty contact region. The weak localization is destroyed by an applied magnetic field and, neglecting spin–orbit coupling, a negative magnetoresistance is expected.

4. Resistance fluctuations

In the magnetoresistance of mesoscopic systems with diffusive electron transport, fluctuations have been observed with a reproducible aperiodic structure [20]. This effect results from the interference between electronic waves traveling phase coherently from one side of the sample to the other. To observe these fluctuations, the condition of phase-coherent transport limits the maximum size of the mesoscopic sample to the inelastic diffusion length. These conductance fluctuations (so-called Universal Conductance Fluctuations) have a universal amplitude e^2/h, which is independent of the size of the sample (however smaller than some dephasing length), independent of the dimensionality and independent of the amount of disorder in the sample [21]. Note that the value e^2/h equals the conductance of just one channel (see Eq. (1)) in the transmission approach of electronic transport. A displacement of one single impurity changes the typical fluctuation pattern in the magnetoresistance (therefore often called "magnetofingerprint"). An applied magnetic field shifts the phases of the electronic waves such that the fluctuations have a typical field scale $B_c \simeq \Phi_0/A$ for a flux quantum $\Phi_0 = h/e$ through the phase-coherent area A of the sample. In the following we will discuss the observation of conductance fluctuations in a ballistic point contact [22].

The fluctuations in the magnetoresistance have been observed in point-contact devices made by nanolithography [8]. These point contacts are very stable and therefore very suitable for an accurate measurement of very small resistance changes. In Fig. 5 the magnetoresistance traces for a Ag point contact show reproducible fluctuations, similar in appearance as Universal Conductance Fluctuations. As a function of the applied bias voltage, the fluctuation pattern changes within 2 meV into a totally different magnetofingerprint. The observed rms amplitude $\delta G \simeq 1.8 \times 10^{-2} e^2/h$ of the conductance fluctuations at zero bias voltage is much smaller than the universal value e^2/h. The half-width of the autocorrelation function for the magnetoresistance yields the characteristic field scale $B_c \simeq 0.07$ of the fluctatuations at zero bias.

The fluctuations in the contact resistance can be explained by quantum interference between the trajectories of ballistically injected electrons and elastically back-scattered electrons. Because of the backlow efficiency a/l_i of the electrons to return back through the contact, a reduced amplitude $(e^2/h)a/l_i$ is found for the fluctuations in a point contact [22]. It should be noted that for a purely ballistic constriction (no scattering with $a/l_i \to 0$) no fluctuations are to be expected. The fluctuation amplitude depends on the size of the contact and the elastic scattering length, in contrast to the universal fluctuations in bulk systems with an isotropic contribution to the diffusive transport. For the device of Fig. 5 we have $a/\ell_i = 5$ nm/240 nm $\simeq 0.02$. The obtained value for the characteristic field B_c

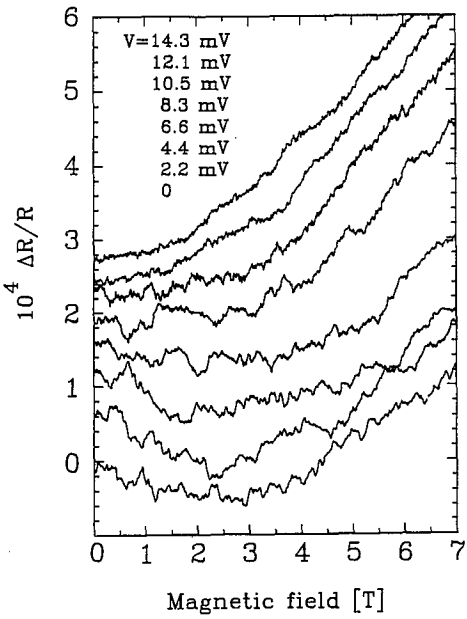

Fig. 5. Fluctuations in the magnetoresistance of a Ag–Ag point-contact device, made by nanolithography, with contact resistance $R = 11\ \Omega$ at 400 mK for different voltages applied over the contact.

supports the model that the size $(\Phi_0/B_c)^{1/2} = 245$ nm of the interference loops contributing to the fluctuations is mainly determined by elastic scattering processes within a scattering length from the orifice.

With an applied voltage over the contact the differentially measured conductance probes the scattering of electrons with an excess energy eV. The excess energy eV (or wavelength) of the electrons influences the interference conditions. The magnetofingerprint changes significantly for a change $E_c = \hbar/t_c$ in the electron energy, where the correlation energy E_c is determined by the time t_c for the electron to pass a phase-coherent region. From the effective length ℓ_i of interfering electron paths contributing to the resistance near the contact, it is found that $E_c = \hbar v_F/\ell_i \simeq 4$ meV. Each time the voltage is changed by $\Delta V \simeq E_c/e$, a new subsystem is entered and hence the magnetofingerprint changes as shown in Fig. 5. The applied voltage (< 10 meV) does not change the amplitude of the oscillations, but only gives access to different coherent subsystems with energy width $\delta E \simeq E_c$.

For larger applied voltages (> 10 mV), in Fig. 5 a decrease in fluctuation amplitude can be observed with an increase in the correlation field B_c. The voltage position of the decease in fluctuation amplitude coincides with the transverse acoustic phonon energy in Ag. The inelastic scattering (via spontaneous emission of phonons) of the electrons destroys the phase coherence along the interference loops. The measured electron–phonon interaction spectrum α^2F on the same contact can be used to determine the energy dependence of the inelastic scattering

length $\ell_{\rm in}(\epsilon)$ (see Eq. (4)). The decrease in fluctuation amplitude can be described by an exponentional factor $\exp(-\ell_{\rm in}({\rm eV})/\ell_{\rm i})$ for the loss of phase coherence along a scattering path length [22]. Once again, this application of ballistic point contacts for the study of interference phenomena in electronic transport shows the possibility to tune the non-equilibrium energy eV of the electrons in a well-defined way by means of the applied voltage.

Acknowledgments

Among my collaborators I would like to thank especially J.A. Kokkedee for his contributions in many of the discussed point-contact studies. We greatly appreciated the co-operation with P.A.M. Holweg, J. Caro and H.A. Verbruggen of the Delft Institute of Microelectronics and Submicron Technology in the investigation of point contacts made with the sophisticated nanofabrication technique.

References

[1] Yu.V. Sharvin, *Zh. Eksp. Teor. Fiz.* **48**, 984 (1965) [*Sov. Phys. JETP* **21**, 655 (1965)].

[2] I.K. Yanson, *Zh. Eksp. Teor. Fiz.* **66**, 1035 (1974) [*Sov. Phys. JETP* **39**, 506 (1974)].

[3] I.K. Yanson, *Fiz. Nizk. Temp.* **9**, 676 (1983) [*Sov. J. Low Temp. Phys.* **9**, 343 (1983)]; I.K. Yanson, O.I. Shklyarevskii, *Fiz. Nizk. Temp.* **12**, 899 (1986) [*Sov. J. Low Temp. Phys.* **12**, 509 (1986)]; I.O. Kulik, A.N. Omel'yanchuk, R.I. Shekhter, *Fiz. Nizk. Temp.* **3**, 1543 (1977) [*Sov. J. Low Temp. Phys.* **3**, 740 (1977)]; A.G.M. Jansen, A.P. van Gelder, P. Wyder, *J. Phys. C, Solid State Phys.* **13**, 6073 (1980); A.M. Duif, A.G.M. Jansen, P. Wyder, *J. Phys., Condens. Matter* **1**, 3157 (1989).

[4] *1st Intern. Conf. on Point-Contact Spectroscopy, September 1991, Kharkov, (Ukraine)* (proceedings to be published in *Fiz. Nizk. Temp. [Sov. J. Low Temp. Phys.]*).

[5] J.C. Maxwell, *A Treatise on Electricity, Magnetism*, Clarendon, Oxford 1904.

[6] R. Landauer, *Philos. Mag.* **21**, 863 (1970); Y. Imry, in: *Directions on Condensed Matter Physics*, Eds. G. Grinstein, G. Mazenko, World Scientific Press, Singapore 1986, p. 101.

[7] A.G.M. Jansen, F.M. Mueller, P. Wyder, *Phys. Rev. B* **16**, 1325 (1977).

[8] K.S. Ralls, R.A. Buhrmann, R.C. Tiberio, *Appl. Phys. Lett.* **55**, 2459 (1989); P.A.M. Holweg, J. Caro, A.H. Verbruggen, S. Radelaar, *Microelectron. Eng.* **11**, 27 (1990).

[9] W.L. McMillan, J.M. Rowell, in: *Superconductivity* Vol. 1, Ed. R.D. Parks, Dekker, New York 1969.

[10] A.I. Akimenko, I.K. Yanson, *Pis'ma Zh. Eksp. Teor. Fiz.* **31**, 209 (1980) [*JETP Lett.* **31**, 191 (1980)].

[11] A.G.M. Jansen, J.H. van de Bosch, H. van Kempen, J.H.J.M. Ribot, P.H.H. Smeets, P. Wyder, *J. Phys. F, Met. Phys.* **10**, 265 (1980).

[12] M. Reiffers, Yu.G. Naidyuk, A.G.M. Jansen, P. Wyder, I.K. Yanson, D. Gignoux, D. Schmitt, *Phys. Rev. Lett.* **62**, 1560 (1989).

[13] M. Pepper, *J. Phys. C, Solid State Phys.* **13**, L709 (1980); **13**, L717 (1980); **13**, L721 (1980).

[14] T. Bever, A. Wieck, K. v. Klitzing, K. Ploog, P. Wyder, *Phys. Rev. B* **44**, 6507 (1991).

[15] B.I. Verkin, I.K. Yanson, I.O. Kulik, O.I. Shklyarevskii, A.A. Lysykh, Yu.G. Naidyuk, *Solid State Commun.* **30**, 215 (1979).

[16] N.N. Gribov, P. Samuely, J.A. Kokkedee, A.G.M. Jansen, P. Wyder, I.K. Yanson, *Phys. Rev. Lett.* **66**, 786 (1991).

[17] I.K. Yanson, N.N. Gribov, O.I. Shklyarevskii, *Pis'ma Zh. Eksp. Teor. Fiz.* **42**, 159 (1985) [*JETP Lett.* **42**, 195 (1985)].

[18] H. Sato, I. Sakamoto, K. Yonemitsu, Y. Hishiyama, *J. Phys. Soc. Jpn.* **57**, 2456 (1988).

[19] P.A. Lee, T.V. Ramakrishnan, *Rev. Mod. Phys.* **57**, 287 (1985).

[20] C.P. Umbach, S. Washburn, R.B. Laibowitz, R.A. Webb, *Phys. Rev. B* **30**, 4048 (1984); W.J. Skocpol, P.M. Mankiewich, R.E. Howard, L.D. Jackel, D.M. Tennant, A.D. Stone, *Phys. Rev. Lett.* **56**, 2865 (1986).

[21] B.L. Altshuler, *Pis'ma Zh. Eksp. Teor. Fiz.* **41**, 530 (1985) [*JETP Lett.* **41**, 648 (1985)]; P.A. Lee, A.D. Stone, *Phys. Rev. Lett.* **55**, 1622 (1985).

[22] P.A.M. Holweg, J.A. Kokkedee, J. Caro, A.H. Verbruggen, S. Radelaar, A.G.M. Jansen, P. Wyder, *Phys. Rev. Lett.* **67**, 2549 (1991).